


Prediction of thermal runaway and thermal management requirements in cylindrical Li-ion cells in realistic scenarios

Krishna Shah^{1,2} | Ankur Jain¹ 

¹Mechanical and Aerospace Engineering Department, University of Texas at Arlington, Arlington, Texas, USA

²Mechanical Engineering Department, University of California at Merced, Merced, California, USA

Correspondence

Ankur Jain, Mechanical and Aerospace Engineering Department, University of Texas at Arlington, Arlington, TX, 500 W First St, Rm 211, Arlington, TX 76019, USA.

Email: jaina@uta.edu

Funding information

National Science Foundation, Grant/Award Number: CBET-1554183

Summary

Li-ion cells suffer from significant safety and performance problems due to overheating and thermal runaway. Effective thermal management can lead to increased energy conversion efficiency and energy storage density. Critical needs towards these goals include the capability to predict thermal behavior in extreme conditions and determine thermal management requirements to prevent thermal runaway. This paper presents an experimentally validated theoretical model to predict the temperature distribution in a cell in response to nonlinear heat generation rate that is known to occur during thermal runaway. This problem is solved by linearization of the nonlinear term over successive time intervals. Experimental measurements carried out on a thermal test cell in conditions similar to thermal runaway show good agreement with the theoretical model. Experimental measurements and model predictions indicate strong dependence of the fate of the cell on its reaction kinetics, thermal properties, and ambient conditions. Specifically, a sudden change in thermal runaway behavior is predicted once the ambient temperature crosses a certain threshold, consistent with past experimental observations. The impact of increasing cell thermal conductivity on improved thermal runaway performance is quantified. Results presented here provide a fundamental understanding of thermal runaway, and may lead to improved performance and safety of Li-ion-based energy conversion and storage systems.

KEYWORDS

battery safety, heat transfer, Li-ion battery cooling, thermal runaway

1 | INTRODUCTION

While Li-ion cells offer several technological advantages for electrochemical energy conversion and storage in multiple applications, the temperature sensitivity of Li-ion cells continues to pose serious concerns related to safety and reliability. Thermal runaway is a widely investigated hazard in electrochemical energy storage systems comprising Li-ion cells.^{1,2} Thermal runaway usually occurs when the cell temperature exceeds a certain threshold, triggering a series of heat-generating decomposition processes and reactions that further increase cell

temperature. This nonlinear phenomenon, where heat generated by one process triggers a new decomposition process that generates even greater amount of heat, eventually leads to fire and catastrophic failure. Thermal runaway is believed to be responsible for several well-publicized product failures in the recent past and therefore has gained much research attention.

The cascade of temperature-sensitive electrochemical reactions responsible for thermal runaway has been well studied.^{1,3-9} Key processes and reactions relevant for thermal runaway include decomposition of solid electrolyte interphase (SEI)⁵, chemical reactions involving

electrolyte and binder,^{6-8,10} decomposition of negative and positive electrodes,¹¹ and decomposition of electrolyte.⁹ Heat generation rates of these exothermic reactions, usually governed by Arrhenius reaction kinetics, have been well studied both theoretically^{3,12,13} and experimentally.^{5,6,14,15} Experimental measurement of reaction rate and heat generation rate has been reported using differential scanning calorimetry and accelerated rate calorimetry.^{5,6,14,15} Temperature measurements during thermal runaway have been reported.^{4,16} Thermal and mechanical abuse has been mimicked in experiments through oven tests,¹⁷⁻¹⁹ short circuit tests,²⁰⁻²² and nail penetration tests.^{23,24}

In comparison to the comprehensive literature available on experimental measurements, relatively lesser work exists on thermal modeling of a Li-ion cell undergoing thermal runaway. Thermal computations has been carried out based on numerical solution schemes^{12,25,26} as well as commercial finite-element software.^{27,28} Thermal abuse modeling that treats the cell as a lumped mass has been reported.^{26,29} One-dimensional²⁵ and three-dimensional^{12,27,28} thermal models have also been developed to simulate thermal runaway in Li-ion cell. Numerical models have also been used for understanding thermal runaway propagation in a battery pack and the effect of cell arrangement in a battery pack.^{19,30}

While numerical models allow for computing temperature fields in a Li-ion cell during thermal runaway, there is clearly a need for developing analytical thermal models that solve the underlying energy conservation equations and provide closed-form solutions to predict whether thermal runaway will occur under realistic conditions. While such an approach is inherently challenging due to the nonlinear nature of thermal runaway, it will provide a computationally efficient and versatile model to predict thermal runaway under a wide range of scenarios. This may help develop tools for real-time monitoring and analyzing effect of heat transfer parameters, including evaluation of thermal runaway prevention strategies. Further, analytical modeling of thermal runaway will help understand the interplay between the crucial physical processes including heat generation, intracell heat conduction, and heat dissipation to the ambient that ultimately governs whether thermal runaway occurs or not. A recent work addresses this important research need by formulating a nondimensional Thermal Runaway Number (TRN) that governs whether thermal runaway is imminent or not.³¹ However, this was a somewhat simplistic approach that assumed a single decomposition reaction, did not account for Arrhenius kinetics, and did not explicitly predict the evolution of cell temperature. The non-dimensional Thermal Runaway Number (TRN) has also been used to predict critical temperature in the Li-ion cell considering different decomposition

reactions.³² Clearly, more comprehensive work needs to be carried out to develop analytical models for predicting temperature fields in a Li-ion cell under abuse conditions.

This paper presents an experimentally validated, analytical thermal model to predict cell temperature as a function of time and therefore predict the transition of a cell from safe operation to the onset of thermal runaway. While thermal modeling of a Li-ion cell has been carried out in past work, the novelty of the present work lies in the capability to account for realistic processes such as multiple decomposition reactions and reactant consumption within the framework of an analytical model. The model solves the governing energy equations that include nonlinear, temperature-dependent heat generation within the cell by piecewise linearizing heat generation rate as a function of temperature. The model is validated through experiments on a thermal test cell subjected to temperature-dependent heat generation. Measurements of the cell temperature as a function of time in these experiments under a variety of heat generation conditions similar to those encountered in thermal runaway of a Li-ion cell are shown to be in good agreement with predictions from the analytical thermal model. It has been shown through the model and validated by experiments that an increase in thermal conductivity results in significant improvement in thermal runaway performance of the cell. The model is also used to analyze the effect of various heat generation, heat transfer, and heat dissipation parameters on the thermal state and temperature of the cell, thereby determining thresholds of these parameters that trigger thermal runaway. Analysis and measurements presented in this work provide fundamental insights into thermal runaway and may form the basis of technologies that predict and mitigate thermal runaway in electrochemical energy storage systems.

2 | MATHEMATICAL MODELING

Consider a cylindrical Li-ion cell of radius R , radial thermal conductivity k_r , and radial thermal diffusivity α_r , shown schematically in Figure 1A. The cell experiences internal heat generation primarily due to Ohmic heat, active polarization heat, and entropic heat during normal operating conditions. The combined heating due to these different mechanisms is defined as the nominal heat generation (Q_N). In addition to nominal heat generation, exothermic heat (Q_E) due to material decomposition is considered under abuse conditions. External cooling due to coolant flow occurs on the outer surface, resulting in a convective heat transfer coefficient h . While Q_N is largely constant, Q_E is, in general, a strong function of temperature due to the Arrhenius nature of the multiple exothermic reactions that occur

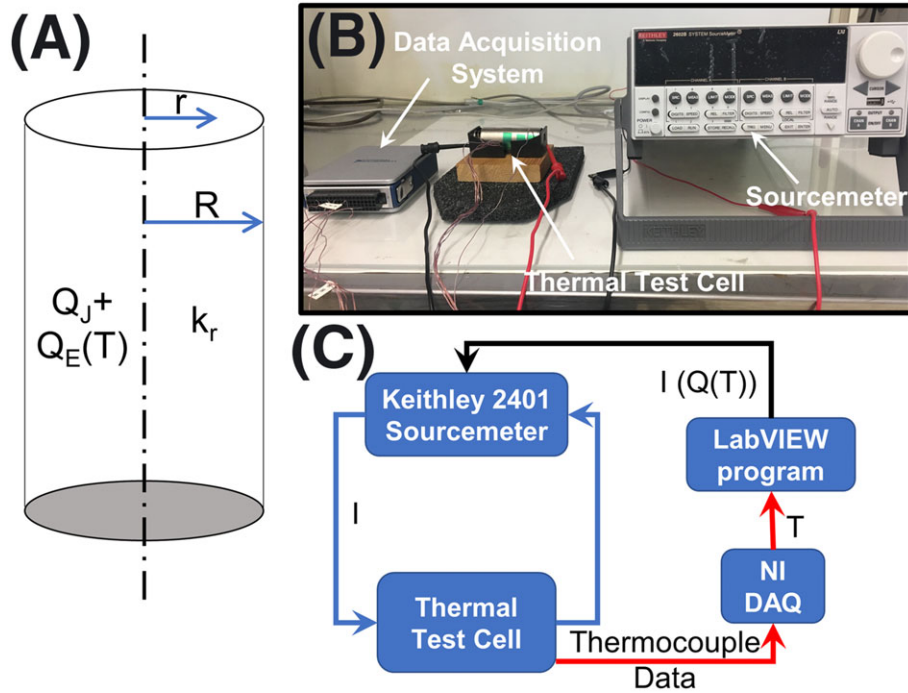


FIGURE 1 A, Schematic of a cylindrical Li-ion cell considered here. B, Experimental setup for validation of thermal model and characterization of thermal behavior of cell under various conditions. C, Schematic showing the mechanism utilized to impose temperature-dependent heat generation in the cell [Colour figure can be viewed at wileyonlinelibrary.com]

in conjunction with each other.³ The interest is in predicting the temperature distribution in the cell as a function of time, and specifically, whether the cell enters thermal runaway. The mathematical modeling of this problem is inherently challenging due to the temperature-dependent heat generation from the exothermic electrochemical reactions, which makes the governing energy equation nonlinear. This problem is solved in an iterative fashion by dividing the time duration of interest into multiple intervals, during each of which, the nonlinear term is suitably linearized. The linearized governing energy equation is solved to compute temperature distribution in each interval. Temperature distribution at the end of an interval is used as the initial temperature distribution for the next interval. In this fashion, temperature distribution for the entire time duration of interest is determined. The governing energy equation for temperature rise $\theta_i(r,t)$ during the i^{th} time interval is given by

$$\left(\frac{\partial^2 \theta_i}{\partial r^2} + \frac{1}{r} \frac{\partial \theta_i}{\partial r}\right) + \frac{Q_N + Q_E}{k_r} = \frac{1}{\alpha_r} \frac{\partial \theta_i}{\partial t} \quad (1)$$

subject to

$$\frac{\partial \theta_i}{\partial r} = 0 \text{ at } r = 0, \quad (2)$$

and

$$-k_r \left(\frac{\partial \theta_i}{\partial r}\right) = h \cdot \theta_i \text{ at } r = R, \quad (3)$$

$$\theta_i = \theta_{0,i}(r) \text{ at } t = 0, \quad (4)$$

where $\theta_{0,i}(r)$ refers to the temperature field at the end of the previous interval, which serves as the initial condition for the present interval. Note that in Equations 1 to 4,

$$\theta_i = T_i - T_\infty \quad (5)$$

where T_i and T_∞ are the temperature field in the cell and the ambient temperature respectively.

As discussed in Section 4.3, multiple decomposition reactions contribute towards the exothermic heat generation term Q_E .³ This is further complicated by reactant consumption during thermal runaway. In order to account for these nonlinear phenomena, Q_E is approximated by a piecewise linear function. By doing so, Equation 1 can be simplified to

$$\left(\frac{\partial^2 \theta_i}{\partial r^2} + \frac{1}{r} \frac{\partial \theta_i}{\partial r}\right) + \frac{Q_N}{k_r} + \frac{\beta_i \cdot (\theta_i + T_\infty)}{k_r} = \frac{1}{\alpha_r} \frac{\partial \theta_i}{\partial t}, \quad (6)$$

where β_i is the coefficient to be multiplied with T_i for piecewise linear approximation of Q_E within the time interval of interest. The coefficient β_i is approximated to be constant throughout the time interval and is computed at the start of the time interval. The duration of the i^{th} time interval is determined based on the deviation of the $\beta_i T_i$ term from the actual exothermic heat generation rate. When this deviation exceeds the specified tolerance, the time interval is reset and the value of β_i is recomputed for the next time

interval. In general, for a given tolerance, the greater the nonlinearity in Q_E , the shorter is each time interval, and hence, the greater is the overall computational cost.

In order to solve Equation 6 for a given time interval, it is noted that heat generation comprises a constant component Q_N , and a temperature-dependent term $\beta_i T_i$, which have fundamentally different impacts on the thermal fate of the cell. The constant component is relatively small and by itself unlikely to lead to thermal runaway. On the other hand, heat generation due to decomposition reactions increases with temperature and therefore may trigger thermal runaway. Specific details of the components of these decomposition reactions, including the effect of reactant consumption, are discussed in Section 4.3. In order to derive a solution for Equation 6 for a general heat generation profile, the solution is written as follows:

$$\theta_i(r, t) = s_i(r) + w_i(r, t), \quad (7)$$

where $s_i(r)$ represents the steady-state component and $w_i(r, t)$ is the remainder. The solution for $s_i(r)$ is derived by combining the general solution with a particular solution, obtained using the method of undetermined coefficients. The solution for the transient component is obtained using the separation of variables method. The resulting solutions for $s_i(r)$ and $w_i(r, t)$ are found to be as follows:

$$s_i(r) = \frac{h \cdot \frac{Q_N}{\beta_i} \cdot J_0 \left(\sqrt{\frac{\beta_i}{k_r}} r \right)}{h \cdot J_0 \left(\sqrt{\frac{\beta_i}{k_r}} R \right) - k_r \sqrt{\frac{\beta_i}{k_r}} \cdot J_1 \left(\sqrt{\frac{\beta_i}{k_r}} R \right)} - \frac{Q_N}{\beta_i}, \quad (8)$$

and

$$w_i(r, t) = \sum_{n=1}^{\infty} C_{i,n} J_0 \left(\frac{\mu_n r}{R} \right) \cdot \exp \left(\alpha \left(\frac{\beta_i}{k_r} - \frac{\mu_n^2}{R^2} \right) \cdot t \right), \quad (9)$$

where J_0 and J_1 are the Bessel functions of the first kind of order 0 and 1 respectively, $C_{i,n}$ are constant coefficients, and μ_n are nondimensional eigenvalues given by the roots of the equation.

$$Bi \cdot J_0(x) - x J_1(x) = 0. \quad (10)$$

Note that $Bi = \frac{hR}{k_r}$ is the Biot number.²⁸

The coefficients $C_{i,n}$ in Equation 9 are obtained using the principle of orthogonality of eigenfunctions and the initial condition for the temperature field during the i^{th} time interval.

$$C_{i,n} = \frac{\int_0^R (-s_i(r) + \theta_{0,i}(r)) \cdot r \cdot J_0 \left(\frac{\mu_n r}{R} \right) dr}{\int_0^R r \cdot J_0^2 \left(\frac{\mu_n r}{R} \right) \cdot dr}. \quad (11)$$

Equations 7 to 9 and 11 represent the final solution for the temperature distribution during the i^{th} time interval. Temperature distribution at the end of this interval is calculated and used as the initial condition for the next time interval, thereby marching forward in time. The deviation between actual value of Q_E and its linearized value in Equation 6 is tracked, in order to determine when the next interval must be considered and β_i must be recomputed.

Time stepping is a key component of this approach that affects the accuracy of temperature prediction. If the time stepping is not small enough, the model might not capture the temperature dependent behavior effectively. This may lead to underestimation in temperature prediction or incorrect prediction of thermal runaway. On the other hand, unnecessarily small-time stepping would increase the computation time significantly without much increase in accuracy. Similarly, the accuracy of piecewise linear approximation in following the exponentially increasing heat generation with temperature also plays a key part in the accuracy of temperature computation. A higher accuracy requires tighter tolerance limit for the linearization, which will be reached more frequently, thereby requiring larger number of time intervals and more frequent computation of the coefficients that appear in the solution. Optimization of both time stepping and piecewise linear approximation has been carried out to ensure minimal computational time without losing accuracy.

3 | EXPERIMENTS

Experimental validation of a thermal runaway model for a Li-ion cell presents several challenges. Accurate measurement and control of heat generation rate and its variation with temperature in real time is not straightforward. Heat generation in abuse conditions in a Li-ion cell occurs due to a variety of decomposition processes. Even though several papers have estimated the reaction kinetics of these processes,^{3,14,27} the heat generation rates are not known exactly and may vary depending on experimental conditions. Further, temperature measurement inside a Li-ion cell during abuse conditions is also not straightforward.³³ Most past research on temperature measurement in a Li-ion cell is limited to the surface temperature,^{18,19} whereas thermal runaway may originate inside the cell where the temperature is higher than the surface.

In order to overcome these experimental difficulties, a thermal test cell is designed and fabricated. The thermal test cell closely matches the geometry and thermal properties of a 26650 Li-ion cell,^{31,34,35} thereby ensuring that experiments are representative of a realistic Li-ion cell undergoing thermal runaway. The thermal test cell also enables close control of temperature-dependent heat generation rate as well as temperature measurement.^{31,34,35} Experiments are carried out at temperatures much lower than actual thermal runaway temperature to ensure safety of the thermal test cell and prevent fire and explosion. The nature of temperature-dependent heat generation used in experiments is the same as in an actual thermal runaway event as expressed by Arrhenius reaction kinetics.³ Therefore, these experiments capture the strong, temperature-dependent dynamics of heat generation in real thermal runaway events, despite the lower temperature in these experiments. This ensures that the nonlinearity of heat generation during thermal runaway is effectively captured in the experiments, while ensuring safety.

3.1 | Fabrication of thermal test cell

The design and fabrication of a thermal test cell used in this work has been described in recent papers.^{31,34,35} In brief, the thermal test cell comprises a tightly wound roll of thin metal foil in a 26650 casing. First, a thin metal foil of thickness 0.025 mm is insulated using Kapton tape, and then wrapped around a thin rod to form a roll with radius and height very close to that of a 26650 Li-ion cell. Seven T-type thermocouples are placed at different lengths on the metal foil, which results in thermocouples at different radii after rolling. To make electrical connection to the metal foil roll, thin metal wires are soldered to the two ends of the metal foil. The roll is then inserted into a metal casing usually used for a 26650 Li-ion cell. The thin rod used for rolling is carefully removed from the casing. A small hole is made in the cap of the casing, through which the heater and thermocouple wires are routed out. In order to fill up air voids inside the cell, it is filled with uncured poly-dimethylsiloxane (PDMS), a commonly used electrically insulating soft polymer. PDMS is then cured for 2 hours at 60°C. PDMS is filled and cured twice in order to ensure complete purging of air. Finally, the test cell is sealed by putting the cap on and securing it with an epoxy. Pictures of the test cell fabrication process may be found in a recent paper.³⁴

Multiple such thermal test cells are fabricated using this process and used for experiments described in subsequent sections. Radial thermal conductivities of these

cells, measured using an adiabatic radial heating method,³⁶ are found to be in 0.20 to 0.25 W/mK range. This is close to the measured thermal conductivity of a 26650 Li-ion cell.³⁶

3.2 | Experiments for temperature-dependent heat generation in thermal test cell

Experiments with temperature-dependent heat generation induced in the thermal test cell are carried out. Figure 1B and 1C show a picture of the experimental setup, and a schematic of the mechanism to induce temperature-dependent heat generation behavior. Electrical current is passed through the metal foil of the thermal test cell using a Keithley 2401 sourcemeter to produce Joule heating. Since the heat generation rate needs to increase with increasing cell temperature in accordance with Arrhenius kinetics, the amount of current passing through the thermal test cell is increased as the cell temperature increases. This is accomplished by temperature measurement through embedded thermocouples using a NI cDAQ 9213 data acquisition unit controlled by LabView software running on a 64 bit computer, followed by changes in the current sourced from the Keithley 2401 sourcemeter, which is also controlled by LabView. The software uses the measured temperature at one second intervals as an input to determine the electrical current required to obtain any desired temperature-dependent heat generation, $Q(T)$, such as an Arrhenius profile with any desired values of activation energy and pre-exponential factor. Potential difference across the metal foil in the thermal test cell is also measured by a Keithley 2100 multimeter in order to precisely measure the heat generation rate in the cell. For safety, experiments are terminated when the cell temperature reaches 55°C. Through this approach, any desired temperature-dependent heat generation, similar to exothermic reactions responsible for thermal runaway in a Li-ion cell, can be imposed on the thermal test cell.

This mechanism to mimic temperature-dependent heat generation has been used in a recent paper on theoretical analysis of thermal runaway.^{31,32}

4 | RESULTS AND DISCUSSION

4.1 | Experimental validation

Temperature-dependent heat generation due to a process governed by Arrhenius kinetics is given by

$$Q(T) = Q_0 \cdot \exp\left(-\frac{E_a}{R_u T}\right), \quad (12)$$

where R_u is the universal gas constant and T is the temperature. Activation energy, E_a , and pre-exponential constant, Q_0 , are the two key Arrhenius parameters that govern temperature-dependent heat generation during thermal runaway in a Li-ion cell. Experiments are carried out to measure peak temperature in the thermal test cell for different values of these parameters and compared against predictions from the analytical thermal model. Figure 2A presents this comparison for different values of activation energy E_a , while Q_0 remains fixed at $1.0 \times 10^{44} \text{ W/m}^3$. There is very good agreement between measurements and analytical model across multiple values of E_a . Similarly, Figure 2B presents results when Q_0 is varied while holding E_a constant at $2.45 \times 10^5 \text{ J/mol}$. Similar to Figure 2A, there is good agreement across the entire range of variations investigated here. A value of $10.5 \text{ W/m}^2\text{K}$ is used for the convective heat transfer coefficient, which is well within the typical range for natural convection. While multiple reactions occur during thermal runaway, only a single reaction is considered here for simplification. This is justified because each of the reactions during thermal runaway is known to follow Arrhenius kinetics,³ which is captured in both experiments and theoretical model shown in Figure 2. A chain of multiple decomposition reactions is implemented next.

4.2 | Modeling multiple reactions

For thermal runaway prediction under realistic conditions, four key electrochemical reactions, namely, SEI decomposition, negative electrode-solvent reaction, positive electrode-solvent reaction, and electrolyte decomposition, are considered for exothermic heat generation.

Effect of separator collapse and resulting internal short circuit has not been considered. This is because ceramic coated separators collapse at a temperature much higher than the onset temperature for thermal runaway.³⁷ Therefore, accounting for separator collapse and resulting internal short circuit are not critical for thermal runaway prediction purposes. Heat generation due to the four key reactions depends on their reaction rate. As a function of temperature T , the total exothermic heat generation is given by³

$$Q_E = W_c H_{\text{sei}} c_{\text{sei}} A_{\text{sei}} e^{\left(\frac{-E_{a_{\text{sei}}}}{R_u T}\right)} + W_c H_{\text{ne}} c_{\text{ne}} e^{\left(\frac{I_{\text{sei}}}{I_{\text{osei}}}\right)} A_{\text{ne}} e^{\left(\frac{-E_{a_{\text{ne}}}}{R_u T}\right)} \\ + W_{\text{pe}} H_{\text{pe}} \alpha_{\text{pe}} (1 - \alpha_{\text{pe}}) A_{\text{pe}} e^{\left(\frac{-E_{a_{\text{pe}}}}{R_u T}\right)} + W_e H_e c_e A_e e^{\left(\frac{-E_{a_e}}{R_u T}\right)} \quad (13)$$

Here, W , H , A , and E_a are amount of active content, reaction heat, frequency factor, and activation energy, respectively. Subscripts denote the corresponding reaction for each term. As these reactions proceed, the participating reactants get consumed and the rate of consumption is governed by a set of ordinary differential equations (ODEs)³

$$\frac{dc_{\text{sei}}}{dt} = -c_{\text{sei}} A_{\text{sei}} e^{\left(\frac{-E_{a_{\text{sei}}}}{R_u T}\right)}, \quad (14)$$

$$\frac{dc_{\text{ne}}}{dt} = -c_{\text{ne}} e^{\left(\frac{I_{\text{sei}}}{I_{\text{osei}}}\right)} A_{\text{ne}} e^{\left(\frac{-E_{a_{\text{ne}}}}{R_u T}\right)}, \quad (15)$$

$$\frac{dt_{\text{sei}}}{dt} = c_{\text{ne}} e^{\left(\frac{I_{\text{sei}}}{I_{\text{osei}}}\right)} A_{\text{ne}} e^{\left(\frac{-E_{a_{\text{ne}}}}{R_u T}\right)}, \quad (16)$$

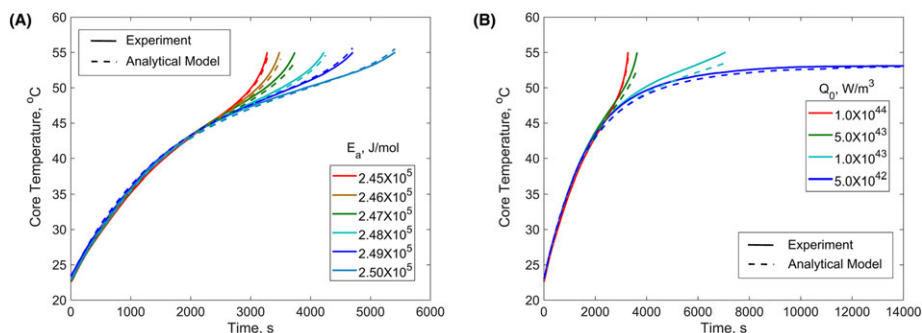


FIGURE 2 A, Comparison of experimental measurement of cell core temperature ($r = 0$) as a function of time with analytical model for different values of activation energy. B, Comparison of experimental measurement of cell core temperature ($r = 0$) as a function of time with analytical model for different values of the preexponential constant. In both cases, good agreement is observed over a range of these parameters [Colour figure can be viewed at wileyonlinelibrary.com]

$$\frac{d\alpha_{pe}}{dt} = \alpha_{pe}(1 - \alpha_{pe})A_{pe}e^{\left(\frac{-E_{a_{pe}}}{R_uT}\right)}, \quad (17)$$

$$\frac{dc_e}{dt} = -c_eA_e e^{\left(\frac{-E_{a_e}}{R_uT}\right)}. \quad (18)$$

Here, c is the nondimensional concentration of reactant in different reactions. As the reactions take place, concentration of reactant decreases and value of c approaches zero. The subscripts here denote the respective reaction. t_{sei} is the thickness of the SEI layer, which increases as the reaction between negative electrode and solvent takes place. Similarly, α_{pe} is the conversion factor which increases to a value of one as the reaction between positive electrode and solvent progresses. More details on these reactions and values of each parameter can be found in the literature.^{3,19,25} The finite difference technique is used to solve the ODEs given by Equations 14 to 18 along with the governing energy equation given by Equation 1.

4.3 | Validation with numerical finite element method solver

In addition to experimental validation, the analytical model is also validated by comparison with finite element simulations. In this case, the effect of heat generation due to four decomposition reactions—SEI decomposition, negative electrode solvent reaction, positive electrode solvent reaction, and electrolyte decomposition—is accounted for. The kinetics of these reactions has been described in past papers^{3,14,33} and is summarized in Equation 13 in Section 4.3. The effect of consumption of participating reactants is captured by well-known ODEs shown in Equations 14 to 18. Under these realistic conditions, Figure 3 shows a comparison of the surface temperature of the cell as a function of time predicted by the model and simulations. In this case, temperature at the surface of the cell is predicted when exposed to a high ambient temperature such as in an oven test. Effect of all four key exothermic electrochemical reactions related to thermal runaway³ is considered. Thermal conductivity and convective heat transfer coefficient are taken to be 0.2 W/mK and 10 W/m²K, respectively. The good agreement between the analytical model and finite-element simulation results, as shown in Figure 3, provides further validation of the analytical model. Although piecewise linearization of heat generation terms is used in the analytical model, it still results in good agreement with finite-element simulations where such linearization has not been done. This clearly shows that the simplification made in the analytical model is not at the expense of accuracy and applicability of the model to capture thermal runaway phenomenon.

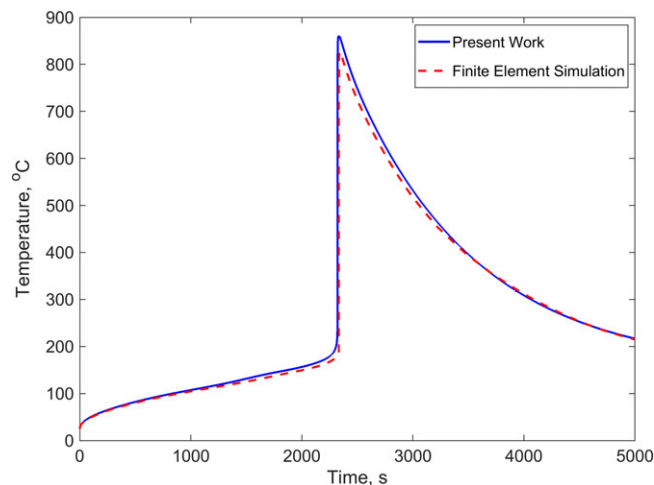


FIGURE 3 Comparison of cell surface temperature as a function of time predicted by the analytical model and finite-element simulations for a 26650 cell undergoing oven test with oven temperature of 150°C and temperature-dependent heat generation corresponding to all four key decomposition reactions [Colour figure can be viewed at wileyonlinelibrary.com]

4.4 | Effect of heat transfer parameters

Effect of heat transfer parameters on thermal behavior of a Li-ion cell is investigated next. Figure 4 presents experimental measurements where temperature-dependent heat generation similar to experiments for Figure 2A and 2B is mimicked in two different thermal test cells. These experiments are carried out in still air, and therefore, heat transfer from the cell to the ambient occurs through natural convection. Similar to Figure 2A and 2B, a value of $h = 10.5$ W/m²K is used for modeling convective heat transfer in the analytical model. The two cells used here, labeled A and B, differ slightly in their construction. While PDMS is poured into cell A during its fabrication, it is not for cell B. Consequently, cell B has air voids inside the casing, resulting in significantly lower thermal conductivity compared with cell A (0.13 W/mK compared with 0.20 W/mK based on measurements). Figure 4, which plots temperature at the cell core ($r = 0$) as a function of time when both cells are subjected to the same temperature-dependent heating, shows dramatically different thermal behavior. While the lower thermal conductivity cell enters thermal runaway, the higher thermal conductivity cell does not. In both cases, there is good agreement between experimental measurements and theoretical model. This highlights the critical importance of thermal conductivity of the cell in preventing thermal runaway and is consistent with a recent paper that showed that thermal conductivity is one of the thermal transport parameters that determines the value of the Thermal Runaway Number (TRN), which in turn governs whether thermal runaway occurs or not.³¹

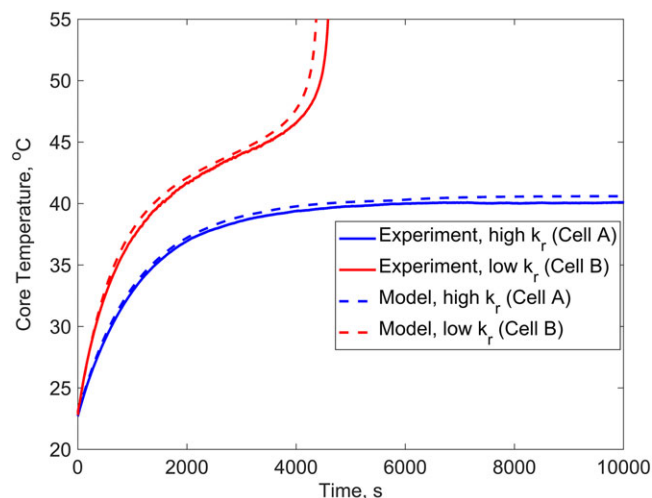


FIGURE 4 Comparison of thermal runaway characteristic of cells with high and low thermal conductivity between experimental measurements and theoretical model prediction of cell core temperature. High thermal conductivity cell is seen to withstand thermal runaway while the low thermal conductivity cell is not [Colour figure can be viewed at [wileyonlinelibrary.com](#)]

There has been much research focus on improving cell thermal conductivity as well as cooling conditions external to the cell. The model discussed in Section 3 can be used to evaluate the effect of such improvements on thermal runaway performance. This is examined in Figure 5. The impact of thermal conductivity on the temperature of the cell is plotted in Figure 5A. These computations use the same thermal conditions as in Figure 4 while accounting for the four key exothermic reactions. Ohmic heating corresponding to a discharge rate of 10C is considered. The temperature plotted in this figure is calculated at $r = R/2$. Figure 5A shows that in this particular case, even a small increase in thermal conductivity can fundamentally change the thermal behavior of the cell from being unstable to stable, thereby avoiding thermal runaway. This is consistent with the experimental demonstration of effect of thermal conductivity on thermal runaway behavior, shown in Figure 4. Such a dramatic impact of thermal conductivity is expected to

occur when the overall thermal resistance of the cell is dominated by the heat conduction resistance within the cell regime. When the cell is not being cooled effectively by external convection, a larger increase in thermal conductivity may be required to influence the thermal runaway behavior of the cell. Some work has been carried out on improving cell thermal conductivity by improving material and interfacial thermal transport.^{38,39} Figure 5A helps evaluate the actual impact of such improvements on the thermal runaway performance of the cell.

Similarly, the effect of convective heat transfer coefficient is also investigated using the experimentally validated thermal model. Using the same heat generation parameters as before, Figure 5B plots temperature at $r = R/2$ in the cell as a function of time for different values of the convective heat transfer coefficient. This figure shows very strong influence of convective heat transfer coefficient on the thermal behavior of the cell. For a given thermal conductivity, heat transfer rate is limited by convective heat transfer coefficient until the coefficient becomes large enough. A small increase in the convection coefficient can increase overall heat dissipation capability of the system, which enables the heat dissipation rate to match up to heat generation rate at higher temperature. This results in change in the thermal behavior of the cell from unstable to stable. Unlike the case of thermal conductivity, a certain minimum increase in convection coefficient leads to prevention of thermal runaway, but a smaller increase does not significantly delay the onset of thermal runaway.

4.5 | Effect of Arrhenius parameters and Ohmic heating

The experimentally validated analytical model is used to examine the effect of changing Arrhenius parameters $E_{a_{sei}}$ and W_c on temperature in a Li-ion cell. Figure 6A presents predicted temperature of the cell at $r = R/2$ as a function of time for different values of $E_{a_{sei}}$ while

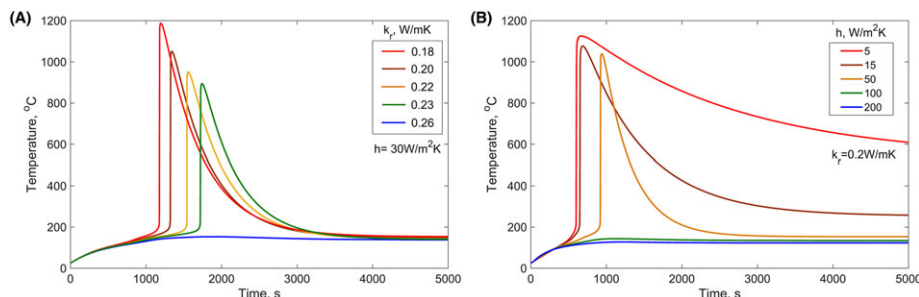
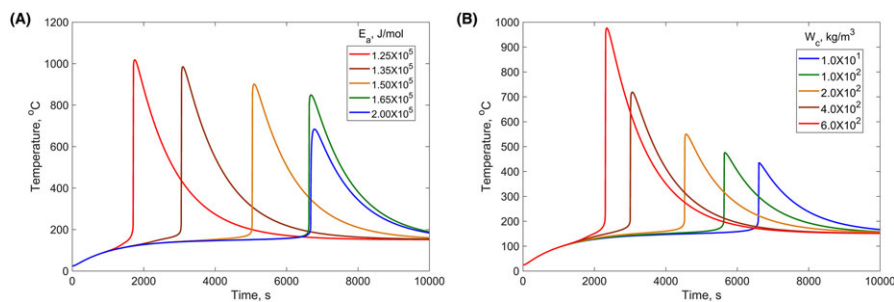


FIGURE 5 Effect of A, radial thermal conductivity, k_r , and B, convective heat transfer coefficient, h , on the thermal runaway characteristics of the cell [Colour figure can be viewed at [wileyonlinelibrary.com](#)]

FIGURE 6 Plot showing the effect of (A) E_a and (B) Q_0 on the temperature of cell at $r = R/2$ as a function of time [Colour figure can be viewed at wileyonlinelibrary.com]



holding rest of the parameters related to the four key decomposition reactions constant. This analysis is carried out considering thermal abuse as the trigger mechanism. Oven temperature of 150°C with convective heat transfer coefficient of $10\text{ W/m}^2\text{K}$ is applied for thermal abuse. Figure 6A shows that increasing $E_{a_{\text{sei}}}$ delays onset of thermal runaway; however, it does not eliminate the risk of thermal runaway. Increasing $E_{a_{\text{sei}}}$ increases the temperature required to initiate the SEI decomposition and negative electrode-solvent reaction, thereby causing delay in the onset of thermal runaway. For $E_{a_{\text{sei}}} > E_{a_{\text{pe}}}$, the positive electrode-solvent reaction would initiate first due to thermal abuse condition ultimately leading to chain of reactions causing thermal runaway. This can be clearly observed from temperature prediction for $E_{a_{\text{sei}}} \geq 1.65 \times 10^5\text{ J/mol}$ in Figure 6A. Here, increasing the $E_{a_{\text{sei}}}$ beyond this value does not delay onset of thermal runaway as the onset temperature is no longer determined by the SEI decomposition or negative electrode-solvent reaction. As soon as the temperature of the cell is sufficiently high to generate enough heat due to the positive electrode-solvent reaction, thermal runaway initiates irrespective of the value of $E_{a_{\text{sei}}}$. These results clearly show that delaying one reaction may not be enough to prevent chain reaction from being initiated. Under the same abuse conditions, effect of change in W_c on the thermal behavior of the cell is shown in Figure 6B. Similar to the effect observed in the previous analysis, reduction in W_c also causes delay in the onset of thermal runaway but does not change the behavior of the cell from unsafe

to safe. The underlying explanation for this is very similar to the one provided to explain the behavior observed in Figure 6A. Although reduction in W_c does not directly change the temperature at which these reactions activate, it has an effect on the amount of heat generated during these reactions at a given temperature. With reduction in W_c , the temperature required for sufficient heating to trigger the chain reaction might be higher, thereby causing delay in the onset of thermal runaway. Also, a large reduction in W_c may help make the cell safer but it would be at the expense of reduced capacity and performance of the cell. Such a tradeoff may not always be acceptable.

Ohmic heating is a key contributor to total heat generation in Li-ion cells during nominal, non-runaway operation. Since this heating is largely temperature-independent and only occurs while the cell is being charged/discharged, it is not the primary mechanism of heat generation responsible for thermal runaway. However, temperature rise due to ohmic heating may activate other electrochemical reactions governed by Arrhenius kinetics, for which heat generation rate rises with temperature, thereby possibly causing thermal runaway. Threshold temperature for such reactions is well known.^{3,14} Figure 7A plots peak temperature as a function of time for Ohmic heating corresponding to different discharge rates. The ohmic heat generation values used in this analysis are taken from previously reported measurements for a 26650 Li-ion cell.⁴⁰ The initial and outside temperature during discharge is fixed

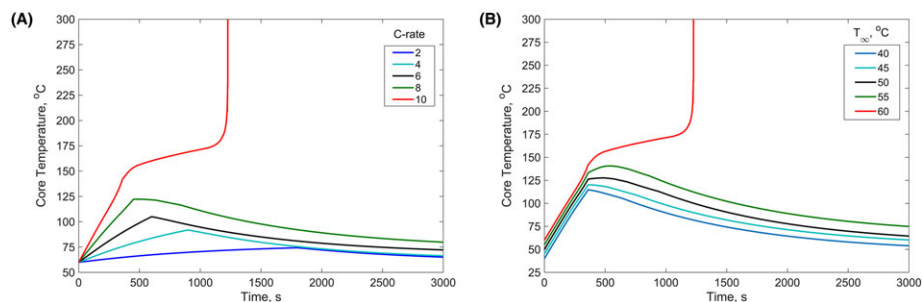


FIGURE 7 Effect of A, Ohmic heating in the cell and B, ambient temperature on cell core temperature as a function of time [Colour figure can be viewed at wileyonlinelibrary.com]

at 60°C for the computations shown in Figure 7A. It can be seen that ohmic heating corresponding to a discharge of 10C causes the cell to enter thermal runaway. This happens primarily because ohmic heating at 10C discharge rate causes large enough temperature rise to trigger the chain of reactions given by Equations 13 to 18, thereby causing thermal runaway.

Figure 7B analyzes the effect of ambient temperature on the cell. Ohmic heating corresponding to a discharge rate of 10C is assumed, and the ambient temperature is varied from 40°C to 60°C in steps of 5°C. Plots for each ambient temperature show that a discharge rate of 10C does not cause enough temperature rise to push the cell into thermal runaway if the ambient temperature is less than 60°C. Once the ambient temperature exceeds around 60°C, however, thermal runaway occurs. This further demonstrates the capability of the present model to predict temperature rise and onset of thermal runaway in practical scenarios. These plots indicate that a combination of extreme ambient conditions and large internal heating within the cell are needed to push the cell into thermal runaway.

4.6 | Thermal response during oven test

The thermal model can also be utilized to predict temperature during oven tests that are commonly used to simulate thermal abuse condition for Li-ion cells and study thermal runaway phenomena. Figure 8 presents peak temperature as a function of time for different ambient temperatures under natural convection conditions. Exothermic heating due to the four key electrochemical reactions occurring during thermal runaway, given by Equations 13 to 18, is used, with no Joule heating. Figure 8 shows that temperature stays bounded until an ambient temperature of about 135°C. At ambient temperature of 140°C, temperature of the cell begins to increase very rapidly, indicating onset of thermal runaway. The existence of such a sharp threshold for the ambient temperature that triggers thermal runaway has also been observed in past experiments.^{18,19,32} Threshold values of the ambient temperature for thermal runaway from these experiments have been observed to be about 150°C, which is close to the predictions from the present work. The small difference in threshold temperature can be due to the use of 18650 cylindrical Li-ion cells, whereas the present work considers 26650 cylindrical cells. Further, other conditions such as convective heat transfer coefficient for the experimental measurements may have been different from the value used in the present work.

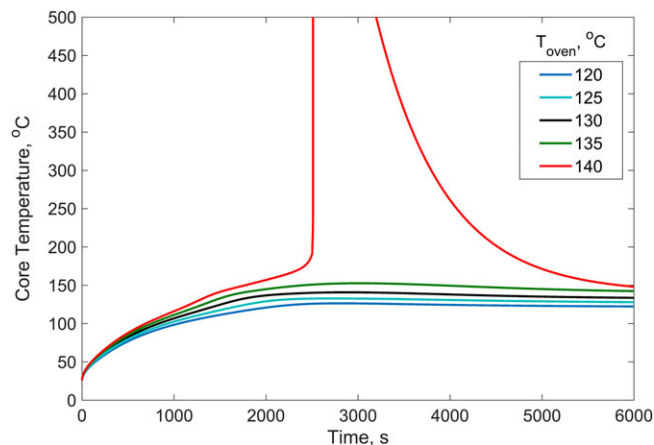


FIGURE 8 Effect of oven temperature (T_{oven}) on the thermal runaway characteristics of the cell during an oven test [Colour figure can be viewed at wileyonlinelibrary.com]

4.7 | Thermal behavior in presence of multiple reactions

Thermal runaway in Li-ion cells is known to be caused by a cascade of exothermic electrochemical reactions that feed into one another and ultimately cause thermal runaway. Figure 9 demonstrates the capability of the analytical model to account for the complicated coupling between multiple temperature-dependent heat generation processes. Figure 9 plots peak temperature as a function of time for four reactions—SEI decomposition, negative solvent reaction, positive solvent reaction, and electrolyte decomposition individually as well as for a situation where all four reactions occur. Recently reported values of the Arrhenius parameters for these processes are used.^{3,14,19,25} None of these reactions lead to thermal runaway individually in the present analysis. However,

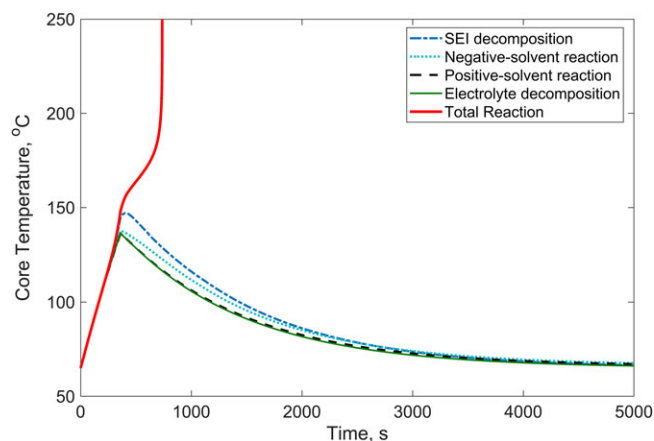


FIGURE 9 Core temperature of the cell as a function of time for four individual heat-generating reactions, as well as for all four reactions combined [Colour figure can be viewed at wileyonlinelibrary.com]

when the total sum of all four reactions is considered, SEI decomposition increases the temperature enough to activate negative electrode solvent reaction and positive electrode solvent reaction which ultimately activates electrolyte decomposition, leading to thermal runaway, as shown in Figure 9. This is indeed the mechanism behind thermal runaway and is well captured by the model shown in Figure 9, which signifies the importance of the cascading effect and the capability of the analytical model to account for the effects of cascading. Note that the behavior of the cell under positive electrode solvent reaction and electrolyte decomposition, as shown in Figure 9, is very similar to each other when considered individually. This is because neither of these two reactions would initiate on their own under the conditions considered in this analysis. Thus, for both the cases, the observed behavior of the cell is only due to the nominal heating considered during the discharge. This further signifies the critical role of the cascading effect of reactions on safety of the cell.

5 | CONCLUSIONS

Thermal runaway is a serious technological challenge that affects the safety and performance of Li-ion cells. This work addresses a key knowledge gap in this field by presenting an experimentally validated model for cell temperature prediction due to nonlinear heat generation in the cell, thereby determining whether thermal runaway will occur or not in given conditions. This is used for identifying the limits of various thermal parameters in order to ensure safety of the cell. Such an approach can be very useful for designing cells to better withstand thermal runaway, as well as run-time thermal management and load balancing in order to prevent thermal runaway during operation. The result that a high thermal conductivity cell is inherently more resistant to the onset of thermal runaway is also potentially of much practical significance, as it may quantify the benefit of thermal conductivity improvement in a Li-ion cell.

It is important to note that the theoretical model does not account for changes in thermal properties of the cell with temperature. Also, a uniformly distributed heat generation rate is assumed, which may not be the case for specific thermal runaway triggers such as internal short circuit. Finally, since the values of the Arrhenius parameters play a key role in model predictions, the model may need to be computed again for other battery chemistries that may have different values of these parameters.

ACKNOWLEDGEMENTS

This material is based upon work supported by CAREER award no. CBET-1554183 from the National Science Foundation.

ORCID

Ankur Jain  <https://orcid.org/0000-0001-5573-0674>

REFERENCES

1. Wang Q, Ping P, Zhao X, Chu G, Sun J, Chen C. Thermal runaway caused fire and explosion of lithium ion battery. *J Power Sources*. 2012;208:210-224.
2. Lisbona D, Snee T. A review of hazards associated with primary lithium and lithium-ion batteries. *Process Saf Environ Prot*. 2011;89(6):434-442.
3. Spotnitz R, Franklin J. Abuse behavior of high-power, lithium-ion cells. *J Power Sources*. 2003;113(1):81-100.
4. Roth EP, Doughty DH. Thermal abuse performance of high-power 18650 Li-ion cells. *J Power Sources*. 2004;128(2):308-318.
5. Richard MN, Dahn JR. Accelerating rate calorimetry study on the thermal stability of lithium intercalated graphite in electrolyte. *J Experimental Electrochem Soc*. 1999;146(6):2068-2077.
6. Maleki H, Deng G, Anani A, Howard J. Thermal stability studies of Li-ion cells and components. *J Electrochem Soc*. 1999;146(9):3224-3229.
7. Du Pasquier A, Disma F, Bowmer T, Gozdz AS, Amatucci G, Tarascon JM. Differential scanning calorimetry study of the reactivity of carbon anodes in plastic Li-ion batteries. *J Electrochem Soc*. 1998;145(2):472-477.
8. Aurbach D, Markovsky B, Salitra G, et al. Review on electrode-electrolyte solution interactions, related to cathode materials for Li-ion batteries. *J Power Sources*. 2007;165(2):491-499.
9. Biensan P, Simon B, Peres JP, et al. On safety of lithium-ion cells. *J Power Sources*. 1999;81:906-912.
10. MacNeil DD, Lu Z, Chen Z, Dahn JR. A comparison of the electrode/electrolyte reaction at elevated temperatures for various Li-ion battery cathodes. *J Power Sources*. 2002;108(1-2):8-14.
11. Roth EP, Nagasubramanian G. *Thermal stability of electrodes in Li-ion cells, Technical Report SAND2000-0345J*. USA: Sandia National Laboratories; 2000.
12. Chen Y, Evans JW. Thermal analysis of lithium-ion batteries. *J Electrochem Soc*. 1996;143(9):2708-2712.
13. Srinivasan V, Wang CY. Analysis of electrochemical and thermal behavior of Li-ion cells. *J Electrochem Soc*. 2003;150(1):A98-A106.
14. Melcher A, Ziebert C, Rohde M, Seifert HJ. Modeling and simulation of the thermal runaway behavior of cylindrical Li-ion cells—computing of critical parameters. *Energies*. 2016;9(4):292.
15. Zhang Z, Fouchard D, Rea JR. Differential scanning calorimetry material studies: implications for the safety of lithium-ion cells. *J Power Sources*. 1998;70(1):16-20.

16. Feng X, Fang M, He X, et al. Thermal runaway features of large format prismatic lithium ion battery using extended volume accelerating rate calorimetry. *J Power Sources*. 2014;255:294-301.
17. Roth EP, Doughty DH, Pile DL. Effects of separator breakdown on abuse response of 18650 Li-ion cells. *J Power Sources*. 2007;174(2):579-583.
18. Golubkov AW, Fuchs D, Wagner J, et al. Thermal-runaway experiments on consumer Li-ion batteries with metal-oxide and olivin-type cathodes. *RSC Adv*. 2014;4(7):3633-3642.
19. Lopez CF, Jeevarajan JA, Mukherjee PP. Characterization of lithium-ion battery thermal abuse behavior using experimental and computational analysis. *J Electrochem Soc*. 2015;162(10):A2163-A2173.
20. Cai W, Wang H, Maleki H, Howard J, Lara-Curzio E. Experimental simulation of internal short circuit in Li-ion and Li-ion-polymer cells. *J Power Sources*. 2011;196(18):7779-7783.
21. Wu MS, Chiang PC, Lin JC, Jan YS. Correlation between electrochemical characteristics and thermal stability of advanced lithium-ion batteries in abuse tests—short-circuit tests. *Electrochim Acta*. 2004;49(11):1803-1812.
22. Santhanagopalan S, Ramadass P, Zhang JZ. Analysis of internal short-circuit in a lithium ion cell. *J Power Sources*. 2009;194(1):550-557.
23. Hatchard TD, Trussler S, Dahn JR. Building a “smart nail” for penetration tests on Li-ion cells. *J Power Sources*. 2014;247:821-823.
24. Maleki H, Howard JN. Internal short circuit in Li-ion cells. *J Power Sources*. 2009;191(2):568-574.
25. Hatchard TD, MacNeil DD, Basu A, Dahn JR. Thermal model of cylindrical and prismatic lithium-ion cells. *J Electrochem Soc*. 2001;148(7):A755-A761.
26. Fang W, Kwon OJ, Wang CY. Electrochemical-thermal modeling of automotive Li-ion batteries and experimental validation using a three-electrode cell. *Int J Energy Res*. 2010;34(2):107-115.
27. Kim GH, Pesaran A, Spotnitz R. A three-dimensional thermal abuse model for lithium-ion cells. *J Power Sources*. 2007;170(2):476-489.
28. Guo G, Long B, Cheng B, Zhou S, Xu P, Cao B. Three-dimensional thermal finite element modeling of lithium-ion battery in thermal abuse application. *J Power Sources*. 2010;195(8):2393-2398.
29. Al Hallaj S, Maleki H, Hong JS, Selman JR. Thermal modeling and design considerations of lithium-ion batteries. *J Power Sources*. 1999;83(1-2):1-8.
30. Smith K, Kim GH, Darcy E, Pesaran A. Thermal/electrical modeling for abuse-tolerant design of lithium ion modules. *Int J Energy Res*. 2010;34(2):204-215.
31. Shah K, Chalise D, Jain A. Experimental and theoretical analysis of a method to predict thermal runaway in Li-ion cells. *J Power Sources*. 2016;330:167-174.
32. Esho I, Shah K, Jain A. Measurements and modeling to determine the critical temperature for preventing thermal runaway in Li-ion cells. *Applied Thermal Engineering*. 2018;145:287-294.
33. Parhizi M, Ahmed MB, Jain A. Determination of the core temperature of a Li-ion cell during thermal runaway. *J Power Sources*. 2017;370:27-35.
34. Shah K, McKee C, Chalise D, Jain A. Experimental and numerical investigation of core cooling of Li-ion cells using heat pipes. *Energy*. 2016;113:852-860.
35. Anthony D, Sarkar D, Jain A. Non-invasive, transient determination of the core temperature of a heat-generating solid body. *Sci Rep*. 2016;6(1):35886.
36. Drake SJ, Wetz DA, Ostanek JK, Miller SP, Heinzl JM, Jain A. Measurement of anisotropic thermophysical properties of cylindrical Li-ion cells. *J Power Sources*. 2014;252:298-304.
37. Orendorff CJ. The role of separators in lithium-ion cell safety. *Electrochem Soc*. 2012;21(2):61-65.
38. Vishwakarma V, Waghela C, Wei Z, et al. Heat transfer enhancement in a lithium-ion cell through improved material-level thermal transport. *J Power Sources*. 2015;300:123-131.
39. Koo B, Goli P, Sumant AV, et al. Toward lithium ion batteries with enhanced thermal conductivity. *ACS Nano*. 2014;8(7):7202-7207.
40. Drake SJ, Martin M, Wetz DA, et al. Heat generation rate measurement in a Li-ion cell at large C-rates through temperature and heat flux measurements. *J Power Sources*. 2015;285:266-273.

How to cite this article: Shah K, Jain A. Prediction of thermal runaway and thermal management requirements in cylindrical Li-ion cells in realistic scenarios. *Int J Energy Res*. 2019;43:1827–1838. <https://doi.org/10.1002/er.4411>